ACSNANO

www.acsnano.org

ARTICLE

Ion Beam Milling as a Symmetry-Breaking Control in the Synthesis of Periodic Arrays of Identically Aligned Bimetallic Janus Nanocrystals

Walker J. Tuff, Robert A. Hughes, Spencer D. Golze, and Svetlana Neretina*

Cite This: *ACS Nano* 2023, 17, 4050–4061

Read Online

ACCESS | Metrics & More | Article Recommendations | Supporting Information

ABSTRACT: **Bimetallic Janus nanostructures represent a highly functional class of nanomaterials due to important physicochemical properties stemming from the union of two chemically distinct metal segments where each maintains a partially exposed surface. Essential to their synthesis is the incorporation of a symmetry-breaking control that is able to induce the regioselective deposition of a secondary metal onto a preexisting nanostructure even though such depositions are, more often than not, in opposition to the innate tendencies of heterogeneous growth modes. Numerous symmetry-breaking controls have been forwarded but the ensuing Janus structure syntheses have not yet achieved anywhere near the same level of control over nanostructure size, shape, and composition as their core−shell and single-element counterparts. Herein, a collimated ion beam is demonstrated as a symmetry-breaking control that allows for the selective removal of a passivating oxide shell from one side of a metal nanostructure to create a configuration that is transformable into a substrate-bound Au−Ag Janus nanostructure. Two different modalities are demonstrated for achieving Janus structures where in one case the oxide dissolves in the growth solution while in the other it remains affixed to form a three-component system. The devised procedures distinguish themselves in their ability to realize complex Janus architectures arranged in periodic arrays where each structure has the same alignment relative to the underlying substrate. The work, hence, provides an avenue for forming precisely tailored Janus structures and, in a broader sense, advances the use of oxides as an effective means for directing nanometal syntheses.**

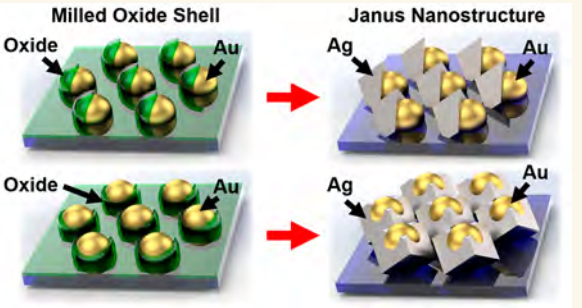

KEYWORDS: *Janus nanoparticle, heterodimer, glancing angle ion milling, symmetry-breaking, regioselective growth, atomic layer deposition*

The design space afforded to inorganic nanostructures has been greatly expanded by the advent of synthetic controls that break crystallographic symmetries and allow for the ordered arrangement of constituent materials.[1−6] Dual-component nanostructure systems with well-defined and uninterrupted interfaces are especially intriguing in this regard in that they form a union between two distinct phases of matter to create single unit nanostructures having components that express different functional properties or which interact to obtain a coupled response that is otherwise unobtainable.[7−12] With inorganic materials exhibiting almost every major physicochemical property, there is a seemingly endless number of opportunities. Within this realm, bimetallic nanostructures are of specific interest because the formation of a metal−metal interface not only combines the distinctive plasmonic, catalytic, and magnetic properties expressed by individual metals but also augments these properties through heteroepitaxial strain, charge transfer, and defect formation.[7−10] When bimetallic nanostructures are formed such that the two metals are connected by a single interface but where each remains partially exposed to the surrounding environment, they are further classified as bimetallic Janus nanostructures.[7−9,13−15] The distinction emphasizes the importance of having readily accessible surfaces in applications that require surface exposure

Received: January 5, 2023
Accepted: February 15, 2023
Published: February 17, 2023

https://doi.org/10.1021/acsnano.3c00149
ACS Nano 2023, 17, 4050−4061

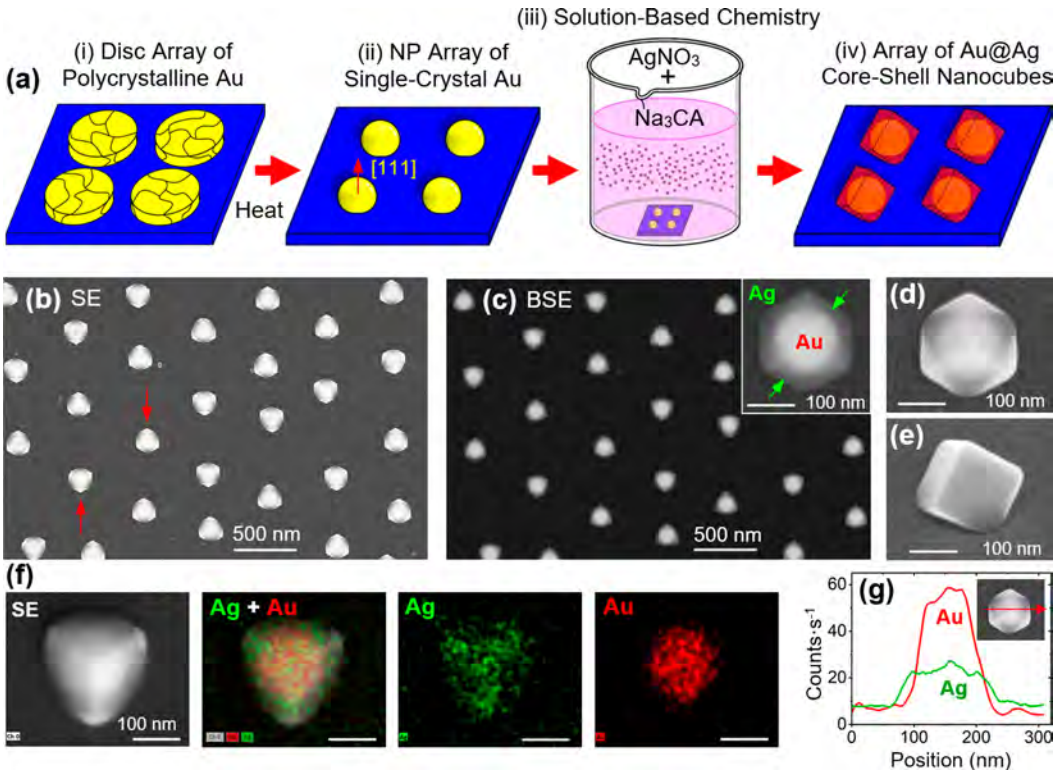

Figure 1. (a) Schematic of the procedure used to form periodic arrays of Au@Ag core−shell nanocubes on [0001]-oriented sapphire substrates. (b) SE and (c) BSE SEM images of the arrayed structures. High-resolution images showing a [111]-oriented nanocube taken from (d) top and (e) tilted views. (f) EDS elemental maps and (g) line scans of a core−shell structure.

to reactants in a catalytic reaction or to analytes in a sensing application. As such, Janus structures have emerged as highly attractive nanomaterials for applications with a scope that includes tandem catalysis, plasmon-enhanced catalysis, strain-induced catalysis, catalytic motors, chemical and biological sensors, bioimaging, theranostics, and anticounterfeiting tags.[7−9,13−17]

Bimetallic Janus nanostructures have been produced as colloids using a diverse collection of techniques.[7−9,14,15] Many of these employ an overall strategy that sees single-component nanostructures separately synthesized and then introduced into a growth solution promoting the deposition of a second metal onto their surface where regioselective controls are put in place to promote the desired side-by-side metal−metal configuration. The strategy is reliant on heterogeneous nucleation onto the presynthesized structures being more favorable than homogeneous nucleation. Symmetry-breaking controls for achieving site-selective heterogeneous growth[2] include the use of (i) slow reduction kinetics capable of triggering growth at a single site after which autocatalytic processes and diffusion ensure continued growth at just that site,[18−21] (ii) twin defects,[19,22] (iii) lattice-mismatch-induced strain,[23−25] (iv) capping agents,[4,21,26−28] (v) nanostructure trapping sites formed at the interface between immiscible liquids where the reduction reaction occurs in just one of the liquids,[29,30] (vi) controlling the reaction stoichiometry in galvanic replacement reactions,[31] (vii) "soft" polymer masks that, when selectively applied, present a barrier to growth while allowing for growth elsewhere,[32−37] and (viii) "hard" inorganic masks that behave similarly.[16,38−42] Among these, the masking techniques provide a conceptually appealing approach and are, in principle, generally applicable. The primary obstacle in forwarding this approach is the application of the mask material in a site-selective manner. Demonstrations that have overcome this hurdle and then gone on to realize bimetallic Janus nanostructures have relied on polystyrene,[32−34,38] polyaniline,[35] poly(styrene-*b*-poly(acrylic acid)),[36,37] and SiO_2[16,39−42] as masking materials. SiO_2 notably stands out as the most widely used and the only one that falls under the category of a hard inorganic mask.

A parallel effort directed toward the formation of bimetallic Janus structures on substrate surfaces presents both opportunities and challenges. Opportunities stem from the integration of wafer-based processing tools into nanofabrication schemes.[43] With a toolset that includes chemical and physical vapor phase depositions, self- and directed-assembly processes, and a wide variety of lithographic techniques, there exist additional avenues for gaining high-level control over nanostructure size, shape, composition, and orientation. Mirkin and co-workers have, for example, devised a scheme for generating periodic arrays of Janus nanostructures based on the coreduction of metal precursors that utilizes scanning-probe block copolymer lithography (SPBCL) in combination with a high-temperature assembly process carried out in a H_2 atmosphere.[44−46] The formation of these substrate-based Janus structures is entirely reliant on phase separation occurring between immiscible components. As such, the procedure is confined to particular metal combinations where few controls exist over shape, the nature of the interface, and the directionality of the structures relative to the underlying substrate. Chen et al.,[47] using a similar growth pathway, examined the phase separation behavior needed to form Au−Rh Janus nanostructures. Other notable achievements include the fabrication of (i) polarization-dependent

https://doi.org/10.1021/acsnano.3c00149
ACS Nano 2023, 17, 4050−4061

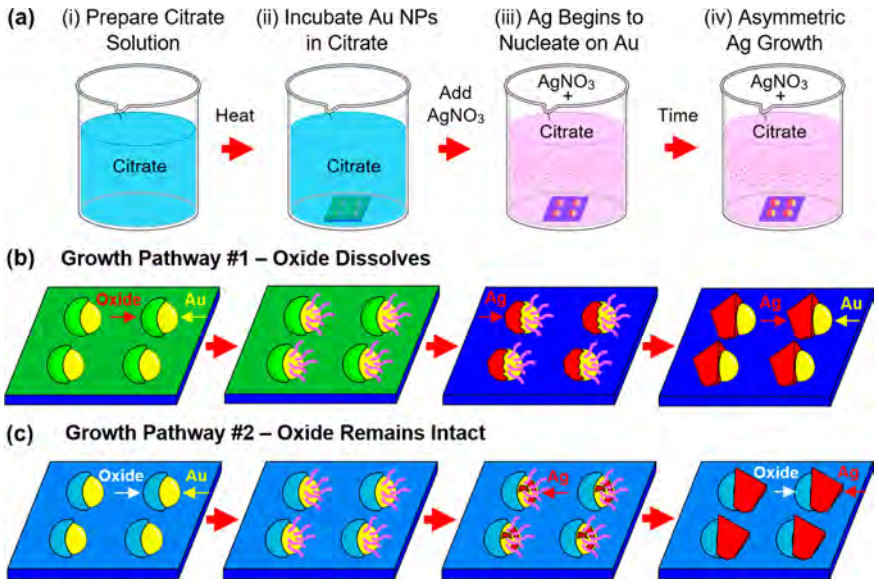

Figure 2. (a) Schematic showing the progression of liquid-state chemical environments that are used to transform Au NPs with a partial oxide coating into a Au−Ag Janus structure. Schematic representations of the structures present on the substrate after each stage for growth pathways where the oxide coating (b) dissolves in the growth solution and (c) remains chemically stable and permanently affixed to the Au. Note that the two growth pathways differ in that Pathway #2 results in oppositely facing Au−Ag Janus structures where the Au segment is encased on all sides.

patterns on glass substrates by forming Au−Ag Janus structures on magnetic nanorods, dispersing them in an acrylamide layer, and then assembling them in a magnetic field so as to simultaneously align both the nanorods and the longitudinal plasmon mode along a chosen direction,[16] and (ii) vertically aligned Ag−M Janus structures (M = Au, Pt, Pd) using a microcontact printing method.[48] Collectively, these demonstrations highlight the distinct nature of substrate-based processing as well as the nanomaterials formed.

With the understanding that seed-mediated colloidal synthesis routes can be practiced on substrate-bound structures,[49] there is opportunity to extend these growth pathways to the formation of bimetallic Janus nanostructures where previously untapped capabilities originate from the use of wafer-based processing tools. Of high relevance are the growth modes utilizing inorganic masks since vapor phase deposition processes provide alternate methods for applying a variety of masking materials while the directional controls offered by glancing angle depositions[50,51] and ion beam milling[52,53] possess the characteristics needed to induce breaks in symmetry. Herein, we demonstrate a strategy for the fabrication of periodic arrays of identically aligned Janus nanostructures that capitalizes on symmetry-breaking capabilities of a collimated ion beam. The overall process sees an oxide mask applied to one side of a metal nanostructure that, when exposed to a suitably chosen liquid-state chemical environment, acts to transform an otherwise symmetric growth mode into one that realizes Janus structures with never-before observed architectures. The work, hence, validates ion milling as a symmetry-breaking control able to promote regioselective growth and provides for significant opportunities in the rational design of metallic nanostructures.

RESULTS

Au@Ag Core−Shell Nanocubes as a Model System. A previously reported Au@Ag core−shell nanocube synthesis[54] is used in this study as a model system for demonstrating two routes that use inorganic masks to redirect its growth along a pathway yielding Au−Ag Janus nanostructures. The procedure for forming core−shell structures, which is shown schematically in Figure 1a, sees a periodic array of substrate-immobilized Au nanoparticles (NPs) formed and then subjected to a liquid-phase synthesis that heterogeneously deposits a (100)-faceted Ag shell onto each of the structures while leaving the exposed sapphire substrate bare. The Au NPs, which ultimately become the core, are formed using a templated dewetting process in which arrays of lithographically defined polycrystalline discs are assembled into [111]-oriented single-crystal structures at elevated temperatures.[55] The Ag shells are formed using a two-reagent seed-mediated synthesis where $AgNO_3$ acts as the Ag^+ precursor and citrate, derived from trisodium citrate (Na_3CA), plays the dual role of capping and reducing agent. Important from the perspective of this work is that the Au cores are incubated in the capping agent for 30 s prior to the onset of the reaction. Shell formation, which is initiated through the injection of aqueous $AgNO_3$, is fairly rapid, requiring only 4 min.

Figure 1b shows a secondary electron (SE) SEM image of a Au@Ag core−shell nanocube array. It shows uniformly sized structures where each is oriented in one of two possible in-plane orientations that differ by 180° (denoted by red arrows). The two orientations originate from two geometrically equivalent heteroepitaxial relationships formed between the (111) planes of Au and the (0001) surface of the sapphire substrate.[56] The backscattered electron (BSE) image, shown in Figure 1c, provides the Z-contrast that clearly reveals the core−shell morphology. Top and tilted view high-magnification images of individual structures (Figure 1d,e) reveal crisp (100) faceting and a nanocube orientation that has its [111]-axis perpendicular to the surface of the substrate. Also noteworthy is that the structure morphology is more accurately described as nanocube-like since it displays an apparent truncation at the Au-substrate interface resulting from the fact that Ag deposition onto the underside of the Au core is

https://doi.org/10.1021/acsnano.3c00149
ACS Nano 2023, 17, 4050−4061

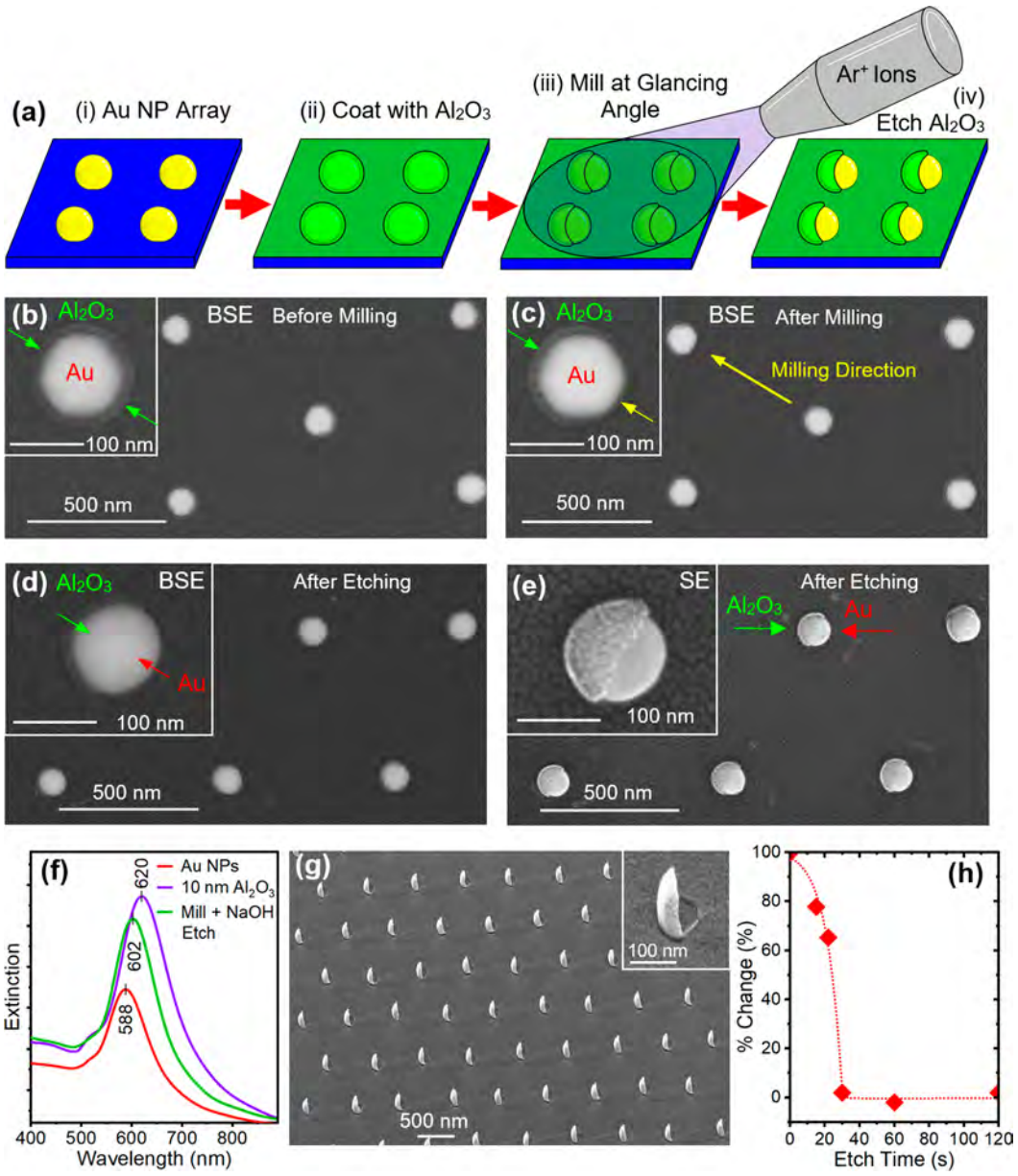

Figure 3. (a) Schematic showing the process by which conformal Al_2O_3 is applied to an array of Au NPs and then selectively removed from one side. BSE SEM images of Au NP arrays that are (b) coated with a 10 nm layer of Al_2O_3, (c) Ar^+ ion milled at a 9° glancing angle, and (d) etched in NaOH to partially expose the Au surface. (e) SE SEM image of a Al_2O_3-coated Au NP array that has undergone the milling/etching procedure. (f) Extinction spectra showing changes to the Au plasmon as the structure is coated with 10 nm of Al_2O_3, milled at a 9° glancing angle, and then etched in NaOH until half the Au surface is exposed. (g) Tilted view SE SEM image of Al_2O_3 shells after the Au component is removed with a selective etch (*i.e.*, *aqua regia*). (h) Time dependence of the percentage shift in the LSPR of Au NPs as a 10 nm thick Al_2O_3 is dissolved in a 10 mM solution of aqueous Na_3CA at 95 °C.

impossible due to the steric barrier imposed by the substrate. Elemental mapping and the associated line scans (Figure 1f,g) derived from energy-dispersive spectroscopy (EDS) measurements confirm the Au@Ag core−shell morphology. Taken together, these results provide an essential comparison when examining the devised pathways for generating Au−Ag Janus nanostructures.

Janus Structure Growth Pathways. Figure 2 shows two growth pathways by which inorganic oxide masks can be used to transform the growth pattern from a Au@Ag core−shell configuration to a Janus structure where the key difference is whether or not the mask dissolves in the growth solution. For both cases, Au NPs are first prepared that have an oxide shell covering half their surface (*vide infra*). They are then subjected to the four-stage progression shown in Figure 2a where the schematic below each (Figure 2b,c) shows a representation of the structures as they would appear at the end of that stage for the two growth pathways. For the first growth pathway (Figure 2b), the shell is designed to be sacrificial by choosing an oxide material that dissolves within the aqueous growth solution on time scales that are small when compared to the duration of the Au@Ag core−shell synthesis (*i.e.*, 3 1/2 min). The partially coated Au structure is first incubated in a growth solution lacking the Ag^+ precursor to allow the time needed for its unprotected surface to become capped with citrate. As this occurs, the sacrificial shell on the other side of the structure

https://doi.org/10.1021/acsnano.3c00149
ACS Nano 2023, 17, 4050−4061

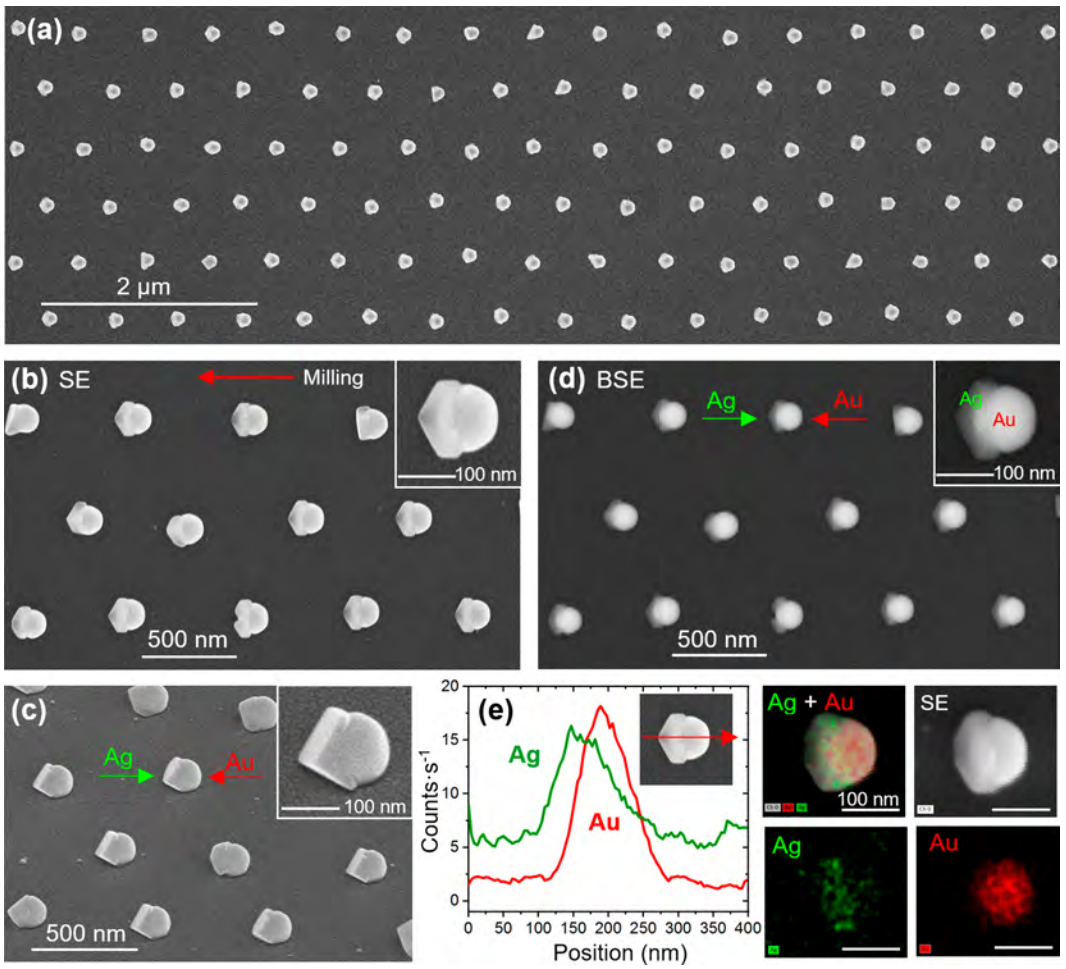

Figure 4. (a) Large-area SEM image of Au−Ag Janus structures. (b) Top and (c) tilted view SEM images of identically aligned Au−Ag Janus structures arranged in periodic arrays. (d) BSE image and (e) EDS elemental line scans and maps that reveal Au and Ag segments arranged in a side-by-side configuration.

begins to dissolve but where it is sufficiently robust to withstand the incubation period. At the onset of the synthesis, brought about by the addition of the aqueous $AgNO_3$, Ag deposition onto the Au structure is inhibited on one side by the oxide and on the other side by the capping agent. This situation is, however, temporary because the dissolution of the oxide eventually exposes the underlying Au to create a surface that is highly favorable for a Ag nucleation event since it is initially free of capping agents. The final product of the reaction is a Au−Ag Janus structure with a side-by-side spatial arrangement where the Ag component expresses (100) faceting. For the second growth pathway (Figure 2c), the oxide shell material is chosen to be chemically inert to the growth solution. The partially coated Au structure is similarly incubated in the citrate capping agent, after which the Ag^+ precursor is added. In this case, Ag^+ reduction onto the Au surface is, once again, inhibited but where the capping agent eventually succumbs to a nucleation event that, in time, gives rise to Ag growth off one side of the structure. The structure is identical with that formed in the first pathway except that it is oppositely facing and exists as a three-component system since the oxide remains permanently affixed to Au. This pathway shares similarities with colloidal Janus structures synthesized utilizing hard inorganic masks.[16,38−42]

Growth Pathway #1 − Oxide Dissolves. The primary challenge in executing the growth pathways presented in Figure 2b,c is the application of an inorganic mask material with the desired functionalities. The process devised for achieving this outcome, which is schematically shown in Figure 3a, begins with the complete encapsulation of the Au NP array within an ultrathin oxide coating. Atomic layer deposition (ALD) is ideally suited for this purpose since it is able to apply conformal pinhole-free oxides where the layer thickness is controlled with monolayer-scale precision.[57] The amorphous nature of these coatings is advantageous because it makes them far more susceptible to etching than their crystalline counterparts. Moreover, the removal of material over time is more uniform since facet-dependent etching processes are absent. Directional modification of the oxide shell is then carried out using a glancing angle milling process that uses a collimated Ar^+ ion beam to selectively thin the oxide on one side of the Au structure while leaving the other side unscathed due to a self-shadowing effect. The entire structure is then exposed to an aqueous etchant for a time interval that allows for the complete removal of the oxide from the milled side while still leaving an oxide shell on the side that is not milled. The overall process, therefore, gives rise to Au NPs that are exposed on one side but not on the other. It should be noted that the milling/etching combination is essential to the success of the

https://doi.org/10.1021/acsnano.3c00149
ACS Nano 2023, 17, 4050−4061

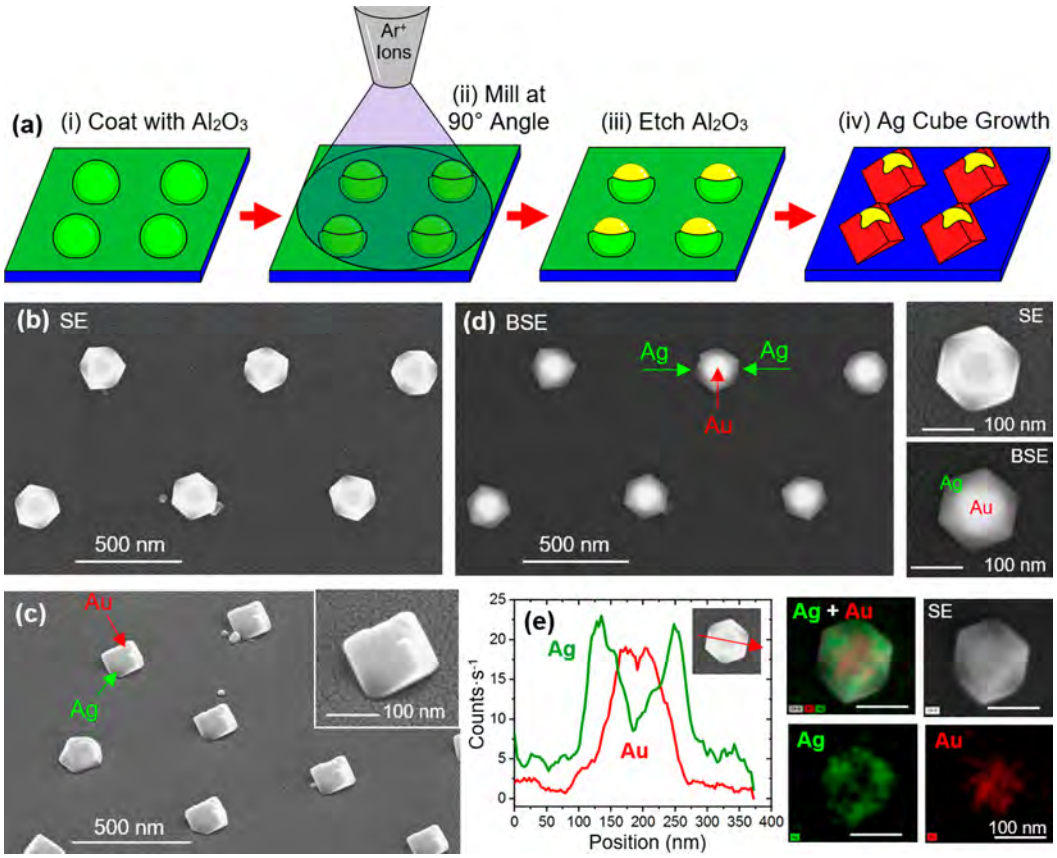

Figure 5. (a) Schematic of the procedure used to form sacrificial Al_2O_3 masks that cover all but the tops of Au NPs arranged in a periodic array as well as the Au−Ag Janus structures that emerge when these masked structures are subjected to a solution-based synthesis. (b) Top and (c) side view SEM images of the arrayed structures. (d) BSE images and (e) EDS elemental line scans and maps that show the spatial distribution of Au and Ag.

process because milling by itself is ineffective since complete oxide removal from one side of the NP gives rise to a damaged Au surface that proves unsatisfactory in the generation of Janus structures.

ALD-deposited Al_2O_3 was selected as the mask material for Janus structures fabricated using Growth Pathway #1. Figure 3b−d shows a progression of three BSE SEM images showing a Au NP array that has been (i) coated with a 10 nm layer of Al_2O_3, (ii) ion milled using a 1.5 keV Ar^+ beam directed at a 9° glancing angle such that one side of the Al_2O_3 shell is selectively thinned, and (iii) exposed to an aqueous NaOH etch for a time interval that is optimized to remove the thinned portion of the Al_2O_3 shell so as to expose the Au NP surface on one side but not the other. Figure 3e shows a SE SEM image of partially encapsulated Au NPs. The application and selective removal of the Al_2O_3 layer was monitored using optical spectroscopy where the localized surface plasmon resonance (LSPR) of the Au structures acts as a built-in sensor responsive to changes in the dielectric environment. Figure 3f shows the extinction spectra taken at various stages of the process. The deposition of 10 nm of Al_2O_3 onto the Au structures causes the plasmon resonance to intensify and red shift from 588 to 620 nm, as is anticipated when the refractive index of the surrounding medium is increased.[57] The milling/etching process leads to a blue shift as well as a significant weakening of the plasmon peak as the dielectric environment surrounding half the Au structure reverts to the uncoated state. Etch tests, which selectively remove the Au component while leaving the Al_2O_3 shell intact followed by SEM characterization, provide further confirmation of the half-shell geometry (Figure 3g and Figure S1). If Al_2O_3 is to act as a sacrificial material in the synthesis of Janus structures, then it is imperative that it dissolves in the Ag nanocube growth solution. Figure 3h provides evidence that this is indeed the case. It presents a plot of the percentage shift in the LSPR of Al_2O_3-coated Au NPs occurring when they are exposed to a growth solution lacking the $AgNO_3$ component for various time intervals. Here, 100% corresponds to the LSPR shift occurring when 10 nm of Al_2O_3 is applied to the Au NPs whereas 0% indicates that the Au NP is oxide-free. The data reveal that the LSPR reverts to its Al_2O_3-free value in approximately 30 s, a time span that is ideal in that it would result in a fresh Au surface being exposed to the growth solution just as the incubation period ends. Collectively, these results confirm that ALD-deposited Al_2O_3 meets the mechanistic requirements needed to enact the growth pathways presented in Figure 2b.

Figure 4a−c shows top and side view SEM images of the structures obtained when an array of Au NPs with sacrificial Al_2O_3 masks are subjected to the solution-based synthesis that yielded the Au@Ag core−shell nanocubes shown in Figure 1. Low-magnification images of larger areas are shown in Figure S2. It is immediately apparent from the SEM data that the mask has a profound influence upon the synthesis, transforming an otherwise symmetric growth pattern into a Au−Ag Janus structure displaying both morphological and compositional breaks in symmetry. Also essential to Janus structure

https://doi.org/10.1021/acsnano.3c00149
ACS Nano 2023, 17, 4050−4061

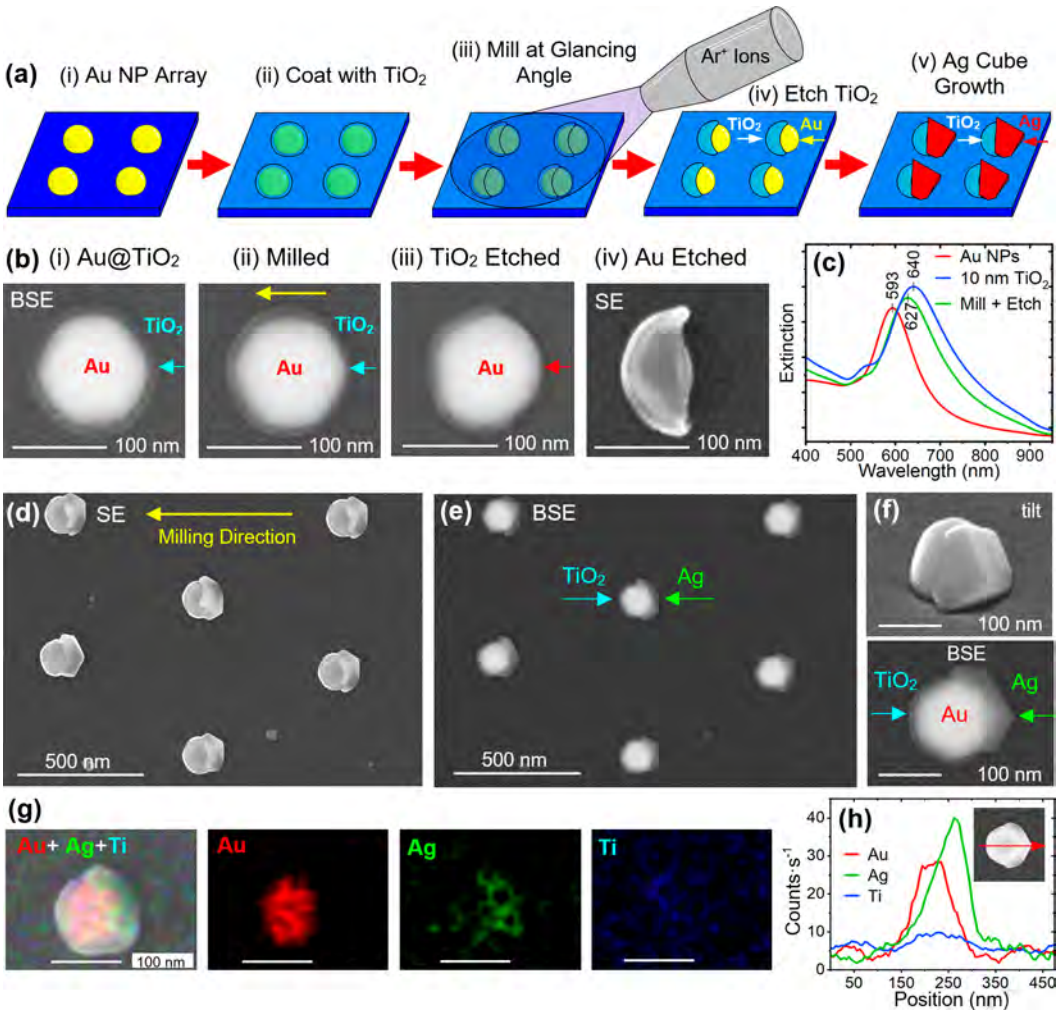

Figure 6. (a) Schematic representation of the process by which a conformal TiO_2 layer is applied to an array of Au NPs, selectively removed from one side, and then transformed into a Janus structure. (b) SEM images showing a progression in which a TiO_2-coated Au NP is ion milled at 9° glancing angle, etched to expose the Au on one side, and then exposed to an etch that removes the Au component. (d) SE and (e) BSE SEM images of a periodic array of Janus structures. (f) High-magnification images of an individual structure where all three components are clearly visible. (g) EDS elemental maps and (h) line scans showing the spatial distribution of the Au, Ag, and Ti components.

formation is the 30 s incubation period in the citrate capping agent prior to the injection of $AgNO_3$ as its elimination gives rise to a core−shell structure. In this scenario, Ag deposition is favorable on the uncapped Au surface (*i.e.*, the milled/etched side) as it enters the reaction and then on masked surface once the Al_2O_3 dissolves.

The Ag component of the Janus structure appears as a nanocube fragment with (100) faceting that emanates in the direction from which the oxide mask was applied (*i.e.*, opposite to the milled/etched side). Such structures have no colloidal analogue. The BSE image and EDS elemental mapping, shown in Figure 4d,e, confirm that the Janus structures are composed of Au and Ag segments arranged in a side-by-side configuration with a well-defined interface. These measurements, however, are unable to establish whether the Al_2O_3 masks were, as expected, consumed in the synthesis. Etch tests, which selectively removed the metal components, established that this was indeed the case as no remnants of the oxide mask were observed. It is also important to appreciate that each structure is identically aligned relative to the underlying substrate where alignment is induced not by lithography but by the directional modification caused by the glancing angle milling process.

A close examination of Growth Pathway #1 reveals that it is dependent on a strong interplay between the (i) oxide thickness, (ii) Ar^+ ion milling time, (iii) incubation time, and (iv) growth parameters associated with the synthesis of the Ag component. Crucial to the pathway is that the milling step leads to a significant thickness difference between the milled and unmilled oxide surfaces. Upon entering into the Ag nanocube growth solution, it is this difference that sets the time interval in which the milled side becomes exposed to the Ag nanocube growth solution while leaving the thicker side temporarily protected. This time interval not only sets the duration of the incubation time but also must be of sufficient duration; otherwise, insufficient capping will occur and lead to Ag growth over the entire Au surface. The product of the reaction will, therefore, be a Au@Ag core−shell structure instead of a Janus structure. A core−shell structure will also emerge if the incubation time is too long because it will allow for both the removal of the entire oxide layer and the efficient capping of the completely exposed Au NP, a scenario that is

https://doi.org/10.1021/acsnano.3c00149
ACS Nano 2023, 17, 4050−4061

equivalent to the Au@Ag nanocube synthesis presented in Figure 1. It should also be understood that the rate of removal of the oxide layer is dependent upon the citrate concentration and temperature used in the Ag synthesis. With these constraints in place, it is essential that the timing of the incubation period be accurately set for the chosen oxide thickness, milling time, and Ag growth parameters.

With the milling process allowing for the site-selective deposition of Ag onto Au NPs, it becomes possible to extend this synthetic strategy by using the milling direction as an adjustable control. In demonstration of this capability, Au−Ag Janus structures were produced using the procedure shown schematically in Figure 5a. It begins by producing sacrificial Al_2O_3 masks using the previously described procedure except that the milling direction is chosen to be normal to the surface of the substrate. The subsequent Al_2O_3 etch in NaOH, therefore, leaves exposed Au on just the top of the structure as is evidenced by etch tests that are analogous to those used to obtain Figure 3g that reveal an array of open-topped Al_2O_3 shells (Figure S3). When such structures are incubated in the aqueous Na_3CA, the exposed Au at the top of each structure becomes capped with citrate as the Al_2O_3 mask begins to dissolve. Complete dissolution, which occurs after the injection of aqueous $AgNO_3$, sees Ag deposited on all the freshly exposed Au surfaces from which the sacrificial mask dissolved but not on those capped by citrate. Figure 5b,c shows top and side view SEM images of the nanostructures produced. As anticipated, the round surface of the central Au structure protrudes from the top of a cube-like Ag shell that encapsulates the rest of the structure. The BSE images and EDS elemental line scans and maps shown in Figure 5d,e, once again, reveal that the Au and Ag components are spatially segregated within the structures. These structures also have no colloidal analogue.

Growth Pathway #2 − Oxide Remains Intact. ALD-deposited TiO_2[57] was selected as the mask material for forwarding the second growth pathway whereby the oxide remains permanently affixed to the Au−Ag Janus structure. Figure 6a shows a schematic of the stepwise procedure in which (i) a Au NP array is prepared, (ii) coated with a 10 nm thick layer of TiO_2, (iii) selectively thinned on one side by glancing angle Ar^+ ion milling, (iv) exposed to a NH_4OH−H_2O_2 etchant for a time interval that removes the TiO_2 remaining on the milled side, and (v) subjected to a Ag nanocube growth solution that allows for growth on the exposed Au surface but not on the areas masked by the TiO_2. Figure 6b shows a progression of BSE SEM images that validate the TiO_2 mask preparation process. They reveal a conformal layer of TiO_2 that is first thinned and then etched to expose the underlying Au. An etch test, which selectively removes the Au, was also carried out to confirm the TiO_2 half-shell geometry. Figures S4 and S5 present images of arrayed structures taken after each step in the progression. Spectroscopic characterization of the mask formation process, as expected, reveals a red shift in the Au plasmon when the TiO_2 layer is applied followed by a blue shift resulting from the TiO_2 milling/etching process (Figure 6c). The chemical stability of ALD-deposited TiO_2 within the Ag nanocube growth solution was verified by the strong spectral overlap occurring in the extinction for TiO_2-coated Au NPs before and after being exposed to a 95 °C growth solution lacking the $AgNO_3$ component (Figure S6) for a time interval that is significantly longer (*i.e.*, 30 min) than that needed for the synthesis of the Ag component (*i.e.*, 4 min).

Figure 6d,e shows SE and BSE SEM images of the structures formed when the TiO_2-masked Au NPs are exposed to the Ag nanocube growth solution. Although these structures appear quite similar to those produced using the Al_2O_3 mask (Figure 4), there is a key difference in that none of the Au is exposed because it is completely encapsulated by a combination of Ag, TiO_2, and the underlying sapphire substrate (Figure 6f). It is also noteworthy that the Ag component forms on the milled side and requires a somewhat longer growth time (4 min as opposed to 3 1/2 min) since the citrate-capped Au surface must be breached. Elemental mapping and the associated line scans (Figure 6g,h) reveal the segmented nature of the Au and Ag components. Overall, these results validate Growth Pathway #2 as a viable route for fabricating Janus structures.

From a mechanistic standpoint, Growth Pathway #2 is far more straightforward. The Au NP enters the Ag nanocube growth with one of its sides exposed while the other is masked with a TiO_2 layer whose surface is chemically inert and unfavorable for Ag deposition. The citrate capping layer formed during the incubation period, while initially inhibiting growth, is eventually breached, after which a nanocube-like growth proceeds. It should be noted that the 30 s incubation step is not vital to this pathway. Eliminating it completely does, however, lead to a somewhat inferior reaction product because there is no time for the room temperature substrate to equilibrate with the 95 °C Ag nanocube growth solution. Incubation times between 10 and 30 s do, however, yield a near-equivalent product.

DISCUSSION

Taken together, the two growth pathways demonstrate the utility of depositing an oxide coating onto a metal NP followed by a directional milling process that results in the formation of an asymmetrically positioned active site for metal deposition. The overall process, referred to as GLAMER (*i.e.*, glancing angle milling, etching, and regrowth), joins a group of substrate-based processing routes that induce nanostructure asymmetries by complimenting lithographic techniques with directed beams that either add or subtract material from the surface.[52,53,58−60] The GLAMER route is distinct from other methods in that it gives rise to complex architectures with a single-crystal character as opposed to polycrystalline structures derived from the physical vapor deposition (PVD) techniques commonly associated with wafer-based processing (*e.g.*, sputtering, evaporation). Other important aspects of the approach include the use of ALD-deposited materials in a manner that exploits differences in chemical stability when compared to metals, the use of an oxide shell as a sacrificial masking material that dissolves in a liquid-state chemical environment, and the integration of wet chemical syntheses into the overall processing route. When compared with leading-edge colloidal routes for preparing Janus structures,[7] the GLAMER process realizes nanostructures that stand out as being among the most sophisticated in terms of architectural complexity. It does, however, have its drawbacks in that the process is somewhat involved, it requires the immobilization of one component of the Janus structure on the substrate surface, the array spacing must be large enough to avoid unwanted shadowing effects during the glancing angle milling process, and selective etch combinations must be established that remove the oxide while leaving the metal components intact. It

https://doi.org/10.1021/acsnano.3c00149
ACS Nano 2023, 17, 4050−4061

should also be noted that the GLAMER process currently yields milled areas of only 3 mm^2 but where this represents a limitation of the instrumentation used rather than an intrinsic constraint placed on the devised process. Notwithstanding, the approach provides a method for forming identically aligned single-crystal bimetallic Janus structures in periodic arrays and, hence, provides an avenue for advancing the synthesis and application of substrate-based nanostructures.

In addition to the formation of bimetallic Janus nanostructures, there exist opportunities to extend the GLAMER strategy beyond dual-component systems. The three-component system obtained using Growth Pathway #2 (Figure 2c), in which the TiO_2 layer remains affixed to the Au component of a Au−Ag Janus structure, provides an initial demonstration in that it combines an oxide material renowned for its light harvesting and photocatalytic capabilities with nanometals.[61] In particular, it is the union of semiconducting and plasmonic components into a single nanostructure architecture that has generated the most interest.[10,11] By using the GLAMER methodology, there is the potential to rationally design multicomponent antenna−reactor photocatalytic systems[62,63] that, for example, combine semiconducting, plasmonic, and Pt-group metals into a single unit expressing sharp interfaces, facets, or even nanogaps supporting intense near-fields. Such capabilities could also prove complementary to an emerging set of techniques for forming periodic arrays of plasmonic dimers held together by molecular linkers that act as a tether between the two NP components.[64−67] Even on the single-element nanostructure level, there exist possible pathways for redirecting otherwise symmetric growth modes with partial oxide shells. We believe that the GLAMER process could prove effective in realizing single element nanostructures that are bimorphic,[68] have internal nanogaps,[69] or express chirality.[70] It could also prove possible to extend the capabilities and viability of this approach by adapting the process to (i) include glancing angle depositions,[51] (ii) produce inorganic oxide shells using the more widely accessible Stöber method,[71] or (iii) use polymer-based shells such as those that have already shown their effectiveness in colloidal syntheses.[32−38]

CONCLUSIONS

In summary, we have demonstrated that ion-beam-induced surface modifications to an oxide-encapsulated Au NP can act as a symmetry-breaking control capable of launching Ag growth trajectories in the deterministic directions needed to form bimetallic Au−Ag Janus nanostructures. The GLAMER process, which is specific to substrate-based structures, capitalizes on the (i) conformal oxide depositions available through the ALD technique, (ii) directional milling capabilities of a collimated ion beam, and (iii) chemically dissimilar properties exhibited by oxides and metals when exposed to etchants and the liquid-state chemical environments required for nanometal syntheses. The so-formed Janus structures distinguish themselves in that they are architecturally complex and formed in periodic arrays where each is identically aligned on the substrate surface. With competencies now demonstrated for the Au−Ag system, this work lays the foundation for advancing a host of regioselective synthetic schemes utilizing various metals and oxides in combination with the rich and diverse liquid-state chemistry dedicated to nanometal syntheses. The potential therefore exists for forming organized surfaces of asymmetric nanomaterials with photonic and chemical properties that are designed to express application-specific responses.

METHODS

Chemicals and Materials. Au NP arrays were fabricated on 10.5 mm × 10 mm × 0.65 mm substrates diced from 100 mm diameter two-side polished wafers of single-crystal [0001]-oriented Al_2O_3 (MTI Corp). The nanoimprint lithography process used a (i) 7030R thermal resist (Micro Resist Technology, GmbH), (ii) PMGI SF 3S liftoff resist, (iii) tetramethylammonium hydroxide solution, 8, III, dioxolane (Kayaku Advanced Materials), (iv) Si nanoimprint lithography stamp (Lightsmyth Technologies), and (v) trichloro-(1*H*,2*H*,2*H*-perfluorooctyl)silane antisticking layer (MilliporeSigma). Au was sputtered from a 19 mm diameter target that was fabricated from a 1.0 mm thick Au foil (99.9985% pure, Alfa Aesar) using a punch and die setup. Dewetting of the Au took place in an ultrahigh-purity Ar gas environment (Airgas). The deposition of the Al_2O_3 and TiO_2 mask materials used trimethylaluminum (TMA) and tetrakis-(dimethylamido)titanium (TDMAT) precursors that were sourced from MilliporeSigma and SAFC Hitech, respectively. Oxide and Au etching solutions were produced from sodium hydroxide (NaOH, Sigma-Aldrich), ammonium hydroxide (28% NH_4OH, Alfa Aesar), hydrogen peroxide (30% H_2O_2, Supelco), nitric acid (HNO_3, Beantown Chemical), and hydrochloric acid (HCl, VWR). Ag cubes were synthesized using trisodium citrate dihydrate ($Na_3C_6H_5O_7{\cdot}2H_2O$, 99% pure, Thermo Scientific) and silver nitrate ($AgNO_3$, reagent ACS, Ward's Science). All solutes were dissolved in deionized (DI) H_2O obtained from a Milli-Q system with a resistivity of 18.2 MΩ·cm.

Periodic Arrays of Au NPs. Arrays were fabricated using a modified version of a previously reported procedure[55] that sees polycrystalline Au discs formed in arrays using nanoimprint lithography followed by a heat treatment that sees each disc assemble into a [111]-oriented single-crystal NP. The nanoimprint lithography process has, however, been modified to include the use of a bilayer resist[72] (*i.e.*, 7030R thermal resist/PMGI SF 3S liftoff resist) that consistently yields a superior product when compared to arrays derived from a single layer resist. The stamp used for nanoimprint lithography consists of an 8 mm × 8.3 mm hexagonal array of cylindrical pillars (350 nm tall, 240 nm diameter) with a center-to-center distance of 600 nm. Once produced, the arrays are typically divided into four pieces where each is used in a separate experiment.

Al_2O_3 Mask Fabrication. Periodic arrays of Au NPs were coated with a 10 nm thick conformal layer of Al_2O_3 using ALD. The deposition proceeds at 200 °C through the repetition of two self-limiting half-reactions brought about by the cyclic introduction of TMA and H_2O precursors into the reaction chamber. Each cycle sees the sequential introduction of two precursors for 20 ms intervals separated by a 7 s N_2 gas purge. Films produced in this manner are amorphous and possess a stoichiometry that is ill-defined. Additional details regarding the ALD depositions, film characterization, and the ellipsometry-based thickness calibration can be found elsewhere.[57] Glancing angle milling was carried out at 9° for 10 s using a collimated 0.55 μA Ar^+ ion beam generated using a 1.5 keV excitation voltage and a gas flow of 0.1 sccm. The remaining Al_2O_3 layer is etched for 4 min in 1 mM aqueous NaOH, rinsed in DI water, and dried in a N_2 gas flow.

TiO_2 Mask Fabrication. TiO_2 mask fabrication proceeded in much the same manner. ALD depositions produced 10 nm thick conformal coatings at 200 °C using TDMAT and H_2O precursors that were cyclically pulsed for 800 ms and 1 s, respectively, where each pulse was separated by a N_2 gas purge time of 7 s and a 3 s pumping interval. Glancing angle milling utilized the same milling angle but where the milling time is increased to 15 s and the excitation voltage is decreased to 0.75 keV. The remaining TiO_2 is etched for 15 s in a solution of 25% NH_4OH, 25% H_2O_2, and 50% DI (by volume).

Ag Synthesis. The Ag component for both the Au@Ag core−shell and Au−Ag Janus structures were produced using a synthesis described in detail elsewhere.[54] It begins with the preparation of 95

https://doi.org/10.1021/acsnano.3c00149
ACS Nano 2023, 17, 4050−4061

°C aqueous solutions of $AgNO_3$ (3 mL, 1 mM) and $Na_3C_6H_5O_7$ (1 mL, 10 mM). The substrate is then incubated in the $Na_3C_6H_5O_7$ for 30 s, after which $AgNO_3$ is added. The Ag nanocube growth is then allowed to proceed for 3 1/2 and 4 min when using the Al_2O_3 and TiO_2 mask, respectively. The substrate is then removed from the solution, sonicated for 5 s in DI water, and dried in air. The sonication step is carried out to remove any loosely bound Ag colloids that spontaneously formed in the growth solution and then inadvertently landed on the nanostructure array.

Etch Tests. Etch tests carried out in demonstration of the integrity of the oxide masks as well as to confirm that the sacrificial Al_2O_3 is consumed in the Ag synthesis placed the sample in *aqua regia* (Hazard: *aqua regia* is highly toxic and corrosive) for 10 min. The substrate is then removed and rinsed in DI H_2O, immediately transferred to acetone, removed, and then gently dried under an N_2 gas flow. Performing the drying step in acetone instead of water reduces the capillary forces that can cause damage to any oxide structures remaining on the substrate surface.

Instrumentation. Nanoimprint lithography utilized a home-built imprinter,[55] a Laurell WS-650-23 B spin coater, and a Samco RIE-1C reactive ion etching system. Au sputter depositions were performed in a Gatan model 681 high-resolution ion beam coater. Au NP assembly was carried out in a Thermo Scientific Lindberg blue/M mini-mite tube furnace equipped with a quartz tube and an Ar flow gas handling system. Al_2O_3 depositions were performed in a Savannah 100 ALD system while TiO_2 depositions were carried out in an Oxford Instrument FlexAL ALD system. A Gatan model 685 PECS II system was used for Ar^+ ion milling. SEM imaging and EDS elemental analysis utilized a Helios G4 UX DualBeam system. Samples were coated with a thin AuPd layer prior to SEM characterization to improve imaging. Extinction spectra were taken in a V-730 UV–visible spectrophotometer.

ASSOCIATED CONTENT

Supporting Information

The Supporting Information is available free of charge at https://pubs.acs.org/doi/10.1021/acsnano.3c00149.

> Figures of SEM images showing periodic arrays of Al_2O_3 and TiO_2 masks after the Au NP component is etched away, large-area SEM images of arrays of Au–Ag Janus structures, SEM and EDS line scans of Au NPs masked with TiO_2, and extinction spectra for standalone and TiO_2-coated Au NPs (PDF)

AUTHOR INFORMATION

Corresponding Author

Svetlana Neretina − *College of Engineering and Department of Chemistry and Biochemistry, University of Notre Dame, Notre Dame, Indiana 46556, United States;* orcid.org/0000-0002-6889-4384; Email: sneretina@nd.edu

Authors

Walker J. Tuff − *College of Engineering, University of Notre Dame, Notre Dame, Indiana 46556, United States*

Robert A. Hughes − *College of Engineering, University of Notre Dame, Notre Dame, Indiana 46556, United States*

Spencer D. Golze − *College of Engineering, University of Notre Dame, Notre Dame, Indiana 46556, United States*

Complete contact information is available at: https://pubs.acs.org/10.1021/acsnano.3c00149

Notes

The authors declare no competing financial interest.

ACKNOWLEDGMENTS

This work was supported by the National Science Foundation, Division of Chemistry, Macromolecular, Supramolecular, and Nanochemistry (MSN) Program under Grant No. CHE–2107728 to S.N. It also benefited from the facilities available through the Notre Dame Integrated Imaging Facility (NDIIF). W.J.T. acknowledges support received through a Notre Dame Materials Science and Engineering Fellowship.

REFERENCES

(1) Nguyen, Q. N.; Wang, C.; Shang, Y.; Janssen, A.; Xia, Y. Colloidal Synthesis of Metal Nanocrystals: From Asymmetrical Growth to Symmetry Breaking. *Chem. Rev.* **2022**.

(2) Yang, X. Q.; Lu, Y.; Liu, Y.; Wang, J.; Shao, L.; Wang, J. F. Heterostructures Built through Site-Selective Deposition on Anisotropic Plasmonic Metal Nanocrystals and Their Applications. *Small Struct* **2021**, *2*, 2100101.

(3) Woessner, Z. J.; Skrabalak, S. E. Symmetry-Reduced Metal Nanostructures Offer New Opportunities in Plasmonics and Catalysis. *J. Phys. Chem. C* **2021**, *125*, 23587–23596.

(4) González-Rubio, G.; Scarabelli, L.; Guerrero-Martinez, A.; Liz-Marzan, L. M. Surfactant-Assisted Symmetry Breaking in Colloidal Gold Nanocrystal Growth. *ChemNanoMat* **2020**, *6*, 698–707.

(5) Huang, Z.; Gong, J.; Nie, Z. Symmetry-Breaking Synthesis of Multicomponent Nanoparticles. *Acc. Chem. Res.* **2019**, *52*, 1125–1133.

(6) Gilroy, K. D.; Peng, H.-C.; Yang, X.; Ruditskiy, A.; Xia, Y. Symmetry Breaking During Nanocrystal Growth. *Chem. Commun.* **2017**, *53*, 4530–4541.

(7) Qiu, J.; Nguyen, Q. N.; Lyu, Z.; Wang, Q.; Xia, Y. Bimetallic Janus Nanocrystals: Syntheses and Applications. *Adv. Mater.* **2022**, *34*, 2102591.

(8) Hoang, K. N. L.; McClain, S. M.; Meyer, S. M.; Jalomo, C. A.; Forney, N. B.; Murphy, C. J. Site-Selective Modification of Metallic Nanoparticles. *Chem. Commun.* **2022**, *58*, 9728–9741.

(9) Ha, M.; Kim, J.-H.; You, M.; Li, Q.; Fan, C.; Nam, J. M. Multicomponent Plasmonic Nanoparticles: From Heterostructured Nanoparticles to Colloidal Composite Nanostructures. *Chem. Rev.* **2019**, *119*, 12208–12278.

(10) Gilroy, K. D.; Ruditskiy, A.; Peng, H.-C.; Qin, D.; Xia, Y. Bimetallic Nanocrystals: Syntheses, Properties, and Applications. *Chem. Rev.* **2016**, *116*, 10414–10472.

(11) Zeng, X.; Zhao, Y.; Hu, X.; Stucky, G. D.; Moskovits, M. Rational Component and Structure Design of Noble-Metal Composites for Optical and Catalytic Applications. *Small Struct* **2021**, *2*, 2000138.

(12) Volokh, M.; Mokari, T. Metal/Semiconductor Interfaces in Nanoscale Objects: Synthesis, Emerging Properties and Applications of Hybrid Nanostructures. *Nanoscale Adv.* **2020**, *2*, 930–961.

(13) Zhang, X.; Fu, Q.; Duan, H.; Song, J.; Yang, H. Janus Nanoparticles: From Fabrication to (Bio)Applications. *ACS Nano* **2021**, *15*, 6147–6191.

(14) Wu, Z.; Li, L.; Liao, T.; Chen, X.; Jiang, W.; Luo, W.; Yang, J.; Sun, Z. Janus Nanoarchitectures: From Structural Design to Catalytic Applications. *Nano Today* **2018**, *22*, 62–82.

(15) Zhang, J.; Grzybowski, B. A.; Granick, S. Janus Particle Synthesis, Assembly, and Application. *Langmuir* **2017**, *33*, 6964–6977.

(16) Feng, J.; Yang, F.; Wang, X.; Lyu, F.; Li, Z.; Yin, Y. Self-Aligned Anisotropic Plasmonic Nanostructures. *Adv. Mater.* **2019**, *31*, 1900789.

(17) Wu, G.-F.; Zhu, J.; Weng, G.-J.; Li, J.-J.; Zhao, J.-W. Heterodimers of Metal Nanoparticles: Synthesis, Properties, and Biological Applications. *Microchimica Acta* **2021**, *188*, 345.

(18) Zhou, L.; Qiu, X.; Lyu, Z.; Zhao, M.; Xia, Y. Pd–Au Asymmetric Nanopyramids: Lateral vs Vertical Growth of Au on Pd Decahedral Seeds. *Chem. Mater.* **2021**, *33*, 5391–5400.

(19) Yang, Y.; Wang, W.; Li, X.; Chen, W.; Fan, N.; Zou, C.; Chen, X.; Xu, X.; Zhang, L.; Huang, S. Controlled Growth of Ag/Au Bimetallic Nanorods through Kinetics Control. *Chem. Mater.* **2013**, *25*, 34−41.
(20) Zeng, J.; Zhu, C.; Tao, J.; Jin, M.; Zhang, H.; Li, Z.-Y.; Zhu, Y.; Xia, Y. Controlling the Nucleation and Growth of Silver on Palladium Nanocubes by Manipulating the Reaction Kinetics. *Angew. Chem.* **2012**, *124*, 2404−2408.
(21) Zhu, C.; Zeng, J.; Tao, J.; Johnson, M. C.; Schmidt-Krey, I.; Blubaugh, L.; Zhu, Y.; Gu, Z.; Xia, Y. Kinetically Controlled Overgrowth of Ag or Au on Pd Nanocrystal Seeds: From Hybrid Dimers to Nonconcentric and Concentric Bimetallic Nanocrystals. *J. Am. Chem. Soc.* **2012**, *134*, 15822−15831.
(22) Lv, T.; Yang, X.; Zheng, Y.; Huang, H.; Zhang, L.; Tao, J.; Pan, L.; Xia, Y. Controlling the Growth of Au on Icosahedral Seeds of Pd by Manipulating the Reduction Kinetics. *J. Phys. Chem. C* **2016**, *120*, 20768−20774.
(23) Liu, J.; Zhang, J. Nanointerface Chemistry: Lattice-Mismatch-Directed Synthesis and Application of Hybrid Nanocrystals. *Chem. Rev.* **2020**, *120*, 2123−2170.
(24) Lyu, Z.; Zhu, S.; Xu, L.; Chen, Z.; Zhang, Y.; Xie, M.; Li, T.; Zhou, S.; Liu, J.; Chi, M.; Shao, M.; Mavrikakis, M.; Xia, Y. Kinetically Controlled Synthesis of Pd−Cu Janus Nanocrystals with Enriched Surface Structures and Enhanced Catalytic Activities toward CO_2 Reduction. *J. Am. Chem. Soc.* **2021**, *143*, 149−162.
(25) Kong, Y.; Zhang, G.; Wang, C.; Ma, Y.; Zheng, Y. Seed Surface Doping-Mediated Seeded growth of Au−Ag Janus Nanoparticles with Tunable Sizes and Multiple Plasmonic Absorption Modes. *CrystEngComm* **2022**, *24*, 6392−6399.
(26) Fan, X.; An, S.; Jia, J.; Xu, W.; Wu, X.; Zong, J.; Wang, Y.; Chen, H.; Feng, Y. Tuning Au−Cu Janus Structures through Strong Ligand-Mediated Interfacial Energy Control. *Chem. Mater.* **2022**, *34*, 6057−6067.
(27) Feng, Y.; Wang, Y.; He, J.; Song, X.; Tay, Y. Y.; Hng, H. H.; Ling, X. Y.; Chen, H. Achieving Site-Specificity in Multistep Colloidal Synthesis. *J. Am. Chem. Soc.* **2015**, *137*, 7624−7627.
(28) Lee, S.-U.; Hong, J. W.; Choi, S.-I.; Han, S. W. Universal Sulfide-Assisted Synthesis of M−Ag Heterodimers (M = Pd, Au, Pt) As Efficient Platforms for Fabricating Metal−Semiconductor Heterostructures. *J. Am. Chem. Soc.* **2014**, *136*, 5221−5224.
(29) Gu, H.; Yang, Z.; Gao, J.; Chang, C.; Xu, B. Heterodimers of Nanoparticles: Formation at a Liquid-Liquid Interface and Particle-Specific Surface Modification by Functional Molecules. *J. Am. Chem. Soc.* **2005**, *127*, 34−35.
(30) Zhang, L.; Wang, Y.; Tong, L.; Xia, Y. Synthesis of Colloidal Metal Nanocrystals in Droplet Reactors: The Pros and Cons of Interfacial Adsorption. *Nano Lett.* **2014**, *14*, 4189−4194.
(31) Kar, N.; McCoy, M.; Zhan, X.; Wolfe, J.; Wang, Z.; Skrabalak, S. E. Reaction Stoichiometry Directs the Architecture of Trimetallic Nanostructures Produced via Galvanic Replacement. *Nanoscale* **2023**.
(32) Qiu, J.; Chen, Z.; Chi, M.; Xia, Y. Swelling-Induced Symmetry Breaking: A Versatile Approach to the Scalable Production of Colloidal Particles with a Janus Structure. *Angew. Chem., Int. Ed.* **2021**, *60*, 12980−12984.
(33) Qiu, J.; Xie, M.; Lyu, Z.; Gilroy, K. D.; Liu, H.; Xia, Y. General Approach to the Synthesis of Heterodimers of Metal Nanoparticles through Site-Selected Protection and Growth. *Nano Lett.* **2019**, *19*, 6703−6708.
(34) Liu, B.; Thanneeru, S.; Lopes, A.; Jin, L.; McCabe, M.; He, J. Surface Engineering of Spherical Metal Nanoparticles with Polymers toward Selective Asymmetric Synthesis of Nanobowls and Janus-Type Dimers. *Small* **2017**, *13*, 1700091.
(35) Xing, S.; Feng, Y.; Tay, Y. Y.; Chen, T.; Xu, J.; Pan, M.; He, J.; Hng, H. H.; Yan, Q.; Chen, H. Reducing the Symmetry of Bimetallic Au@Ag Nanoparticles by Exploiting Eccentric Polymer Shells. *J. Am. Chem. Soc.* **2010**, *132*, 9537−9539.
(36) Woessner, Z. J.; Lewis, G. R.; Bueno, S. L. A.; Ringe, E.; Skrabalak, S. E. Asymmetric Seed Passivation for Regioselective Overgrowth and Formation of Plasmonic Nanobowls. *Nanoscale* **2022**, *14*, 16918.
(37) Wang, Z.; He, B.; Xu, G.; Wang, G.; Wang, J.; Feng, Y.; Su, D.; Chen, B.; Li, H.; Wu, Z.; Zhang, H.; Shao, L.; Chen, H. Transformable Masks for Colloidal Nanosynthesis. *Nat. Comm* **2018**, *9*, 563.
(38) Duan, H.; Malesky, T.; Wang, J.; Liu, C.-H.; Tan, H.; Nieh, M.-P.; Lin, Y.; He, J. Patchy Metal Nanoparticles with Polymers: Controllable Growth and Two-Way Self-Assembly. *Nanoscale* **2022**, *14*, 7364−7371.
(39) Crane, C. C.; Tao, J.; Wang, F.; Zhu, Y.; Chen, J. Mask-Assisted Seeded Growth of Segmented Metallic Heteronanostructures. *J. Phys. Chem. C* **2014**, *118*, 28134−28142.
(40) Hu, Y.; Liu, Y.; Li, Z.; Sun, Y. Highly Asymmetric, Interfaced Dimers Made of Au Nanoparticles and Bimetallic Nanoshells: Synthesis and Photo-Enhanced Catalysis. *Adv. Funct. Mater.* **2014**, *24*, 2828−2836.
(41) Wang, F.; Cheng, S.; Bao, Z.; Wang, J. Anisotropic Overgrowth of Metal Heterostructures Induced by a Site-Selective Silica Coating. *Angew. Chem.* **2013**, *125*, 10534−10538.
(42) Chen, T.; Chen, G.; Xing, S.; Wu, T.; Chen, H. Scalable Routes to Janus Au-SiO_2 and Ternary Ag-Au-SiO_2 Nanoparticles. *Chem. Mater.* **2010**, *22*, 3826−3828.
(43) Hughes, R. A.; Menumerov, E.; Neretina, S. When Lithography Meets Self-Assembly: A Review of Recent Advances in the Directed Assembly of Complex Metal Nanostructures on Planar and Textured Surfaces. *Nanotechnology* **2017**, *28*, 282002.
(44) Chen, P.-C.; Liu, M.; Du, J. S.; Meckes, B.; Wang, S.; Lin, H.; Dravid, V. P.; Wolverton, C.; Mirkin, C. A. Interface and Heterostructure Design in Polyelemental Nanoparticles. *Science* **2019**, *363*, 959−964.
(45) Chen, P.-C.; Liu, X.; Hedrick, J. L.; Xie, Z.; Wang, S.; Lin, Q.-Y.; Hersam, M. C.; Dravid, V. P.; Mirkin, C. A. Polyelemental Nanoparticle Libraries. *Science* **2016**, *352*, 1565−1569.
(46) Huang, L.; Shen, B.; Lin, H.; Shen, J.; Jibril, L.; Zheng, C. Y.; Wolverton, C.; Mirkin, C. A. Regioselective Deposition of Metals on Seeds within a Polymer Matrix. *J. Am. Chem. Soc.* **2022**, *144*, 4792−4798.
(47) Chen, P.-C.; Gao, M.; Yu, S.; Jin, J.; Song, C.; Salmeron, M.; Scott, M. C.; Yang, P. Revealing the Phase Separation Behavior of Thermodynamically Immiscible Elements in a Nanoparticle. *Nano Lett.* **2021**, *21*, 6684−6689.
(48) Zhang, Q.; Lee, Y. H.; Phang, I. Y.; Pedireddy, S.; Tjiu, W. W.; Ling, X. Y. Bimetallic Platonic Janus Nanocrystals. *Langmuir* **2013**, *29*, 12844−12851.
(49) Neretina, S.; Hughes, R. A.; Gilroy, K. D.; Hajfathalian, M. Noble Metal Nanostructure Synthesis at the Liquid−Substrate Interface: New Structures, New Insights, and New Possibilities. *Acc. Chem. Res.* **2016**, *49*, 2243−2250.
(50) Hawkeye, M. M.; Brett, M. J. Glancing Angle Deposition: Fabrication, Properties, and Applications of Micro- and Nanostructured Thin Films. *J. Vac. Sci. Technol. A* **2007**, *25*, 1317−1335.
(51) Zhao, Y.; Ye, D.; Wang, G.; Lu, T. Designing Nanostructures by Glancing Angle Deposition. *P. Soc. Photo-Opt. Ins.* **2003**, *5219*, 59−73.
(52) King, N. S.; Li, Y.; Ayala-Orozco, C.; Brannan, T.; Nordlander, P.; Halas, N. J. Angle- and Spectral-Dependent Light Scattering from Plasmonic Nanocups. *ACS Nano* **2011**, *5*, 7254−7262.
(53) Choi, Y.; Hong, S.; Lee, L. P. Shadow Overlap Ion-Beam Lithography for Nanoarchitectures. *Nano Lett.* **2009**, *9*, 3726−3731.
(54) Hajfathalian, M.; Gilroy, K. D.; Hughes, R. A.; Neretina, S. Citrate-Induced Nanocubes: A Reexamination of the Role of Citrate As a Shape−Directing Capping Agent for Ag-Based Nanostructures. *Small* **2016**, *12*, 3444−3452.
(55) Menumerov, E.; Golze, S. D.; Hughes, R. A.; Neretina, S. Arrays of Highly Complex Noble Metal Nanostructures using Nanoimprint Lithography in Combination with Liquid-Phase Epitaxy. *Nanoscale* **2018**, *10*, 18186−18194.
(56) Golze, S. D.; Hughes, R. A.; Menumerov, E.; Rouvimov, S.; Neretina, S. Synergistic Roles of Vapor- and Liquid-Phase Epitaxy in

https://doi.org/10.1021/acsnano.3c00149
ACS Nano 2023, 17, 4050−4061

the Seed-Mediated Synthesis of Substrate-Based Noble Metal Nanostructures. *Nanoscale* **2021**, *13*, 20225−20233.
(57) Preston, A. S.; Hughes, R. A.; Demille, T. B.; Neretina, S. Plasmonics under Attack: Protecting Copper Nanostructures from Harsh Environments. *Chem. Mater.* **2020**, *32*, 6788−6799.
(58) Ai, B.; Zhao, Y. Glancing Angle Deposition Meets Colloidal Lithography: A New Evolution in the Design of Nanostructures. *Nanophotonics* **2018**, *8*, 1−26.
(59) Shao, L.; Zheng, J. Fabrication of Plasmonic Nanostructures by Hole-Mask Colloidal Lithography: Recent Development. *Appl. Mater. Today* **2019**, *15*, 6−17.
(60) Fredriksson, H.; Alaverdyan, Y.; Dmitriev, A.; Langhammer, C.; Sutherland, D. S.; Zäch, M.; Kasemo, B. Hole−Mask Colloidal Lithography. *Adv. Mater.* **2007**, *19*, 4297−4302.
(61) Kumar, A.; Choudhary, P.; Kumar, A.; Camargo, P. H. C.; Krishnan, V. Recent Advances in Plasmonic Photocatalysis Based on TiO_2 and Noble Metal Nanoparticles for Energy Conversion, Environmental Remediation, and Organic Synthesis. *Small* **2022**, *18*, 2101638.
(62) Halas, N. J. Introductory lecture: Hot-Electron Science and Microscopic Processes in Plasmonics and Catalysis. *Faraday Discuss.* **2019**, *214*, 13−33.
(63) Jain, V.; Kashyap, R. K.; Pillai, P. P. Plasmonic Photocatalysis: Activating Chemical Bonds through Light and Plasmon. *Adv. Optical Mater.* **2022**, *10*, 2200463.
(64) Ye, S.; Zha, H.; Xia, Y.; Dong, W.; Yang, F.; Yi, C.; Tao, J.; Shen, X.; Yang, D.; Nie, Z. Centimeter-Scale Superlattices of Three-Dimensionally Orientated Plasmonic Dimers with Highly Tunable Collective Properties. *ACS Nano* **2022**, *16*, 4609−4618.
(65) Yang, F.; Ye, S.; Dong, W.; Zheng, D.; Xia, Y.; Yi, C.; Tao, J.; Sun, C.; Zhang, L.; Wang, L.; Chen, Q.; Wang, Y.; Nie, Z. Laser-Scanning-Guided Assembly of Quasi-3D Patterned Arrays of Plasmonic Dimers for Information Encryption. *Adv. Mater.* **2021**, *33*, 2100325.
(66) Lin, Q.-Y.; Mason, J. A.; Li, Z.; Zhou, W.; O'Brien, M. N.; Brown, K. A.; Jones, M. R.; Butun, S.; Lee, B.; Dravid, V. P.; Aydin, K.; Mirkin, C. A. Building Superlattices from Individual Nanoparticles via Template-Confined DNA-Mediated Assembly. *Science* **2018**, *359*, 669−672.
(67) Laxminarayana, G. K.; Rozin, M.; Smith, S.; Tao, A. R. Modular, Polymer-Directed Nanoparticle Assembly for Fabricating Metamaterials. *Faraday Discuss.* **2016**, *186*, 489−502.
(68) Cathcart, N.; Kitaev, V. Symmetry Breaking by Surface Blocking: Synthesis of Bimorphic Silver Nanoparticles, Nanoscale Fishes and Apples. *Sci. Rep.* **2016**, *6*, 32561.
(69) Kim, J. M.; Lee, C.; Lee, Y.; Lee, J.; Park, S.-J.; Park, S.; Nam, J.-M. Synthesis, Assembly, Optical Properties, and Sensing Applications of Plasmonic Gap Nanostructures. *Adv. Mater.* **2021**, *33*, 2006966.
(70) Golze, S. D.; Porcu, S.; Zhu, C.; Sutter, E.; Ricci, P. C.; Kinzel, E. C.; Hughes, R. A.; Neretina, S. Sequential Symmetry-Breaking Events As a Synthetic Pathway for Chiral Gold Nanostructures with Spiral Geometries. *Nano Lett.* **2021**, *21*, 2919−2925.
(71) Li, W.; Zhao, D. Extension of the Stöber Method to Construct Mesoporous SiO_2 and TiO_2 Shells for Uniform Multifunctional Core-Shell Structures. *Adv. Mater.* **2013**, *25*, 142−149.
(72) Nagel, R. D.; Filser, S.; Zhang, T.; Manzi, A.; Schönleber, K.; Lindsly, J.; Zimmermann, J.; Maier, T. L.; Scarpa, G.; Krischer, K.; Lugli, P. Nanoimprint Methods for the Fabrication of Macroscopic Plasmonically Active Metal Nanostructures. *J. Appl. Phys.* **2017**, *121*, 084305.

https://doi.org/10.1021/acsnano.3c00149
ACS Nano 2023, 17, 4050−4061